Atmospheric Correction Using the Information from the Short Blue Band

Menghua Wang and Lide Jiang

***Abstract*—We describe our effort to use normalized water-leaving radiance at the short blue band 410 nm, $nL_w(410)$, derived from the Visible Infrared Imaging Radiometer Suite (VIIRS) onboard the Suomi National Polar-orbiting Partnership (SNPP) to improve the VIIRS ocean color products over coastal and inland waters, in particular, over the regions contaminated by strongly absorbing aerosols. The current standard atmospheric correction algorithm has significant issues when dealing with cases of strongly absorbing aerosols, e.g., dust, smoke, air pollution from nearby cities, etc. For such cases, satellite-derived normalized water-leaving radiance spectra $nL_w(\lambda)$ are usually biased low and may be negative, particularly for the short blue bands, e.g., for the VIIRS $nL_w(410)$. In addition, for extremely turbid waters and waters dominated by colored dissolved organic matter (CDOM) that is strongly absorbing at the short blue band, slightly negative $nL_w(410)$ data are also sometimes observed. Obviously, cases with $nL_w(410) < 0$ are unphysical and incorrect. However, VIIRS-derived $nL_w(410) < 0$ do provide useful information to further improve satellite-derived ocean color products in such cases. In this paper, we develop a technique to improve VIIRS ocean color products in cases with strongly absorbing aerosols, CDOM-dominated and extremely turbid waters using VIIRS-derived $nL_w(410)$ information. Specifically, for cases with $nL_w(410) < 0$, atmospheric correction can be carried out again to ensure that $nL_w(410) \geq 0$ (e.g., assuming $nL_w(410) = 0$), thereby removing unphysical retrievals for VIIRS-derived $nL_w(\lambda)$ spectra. Using this technique, VIIRS-derived $nL_w(\lambda)$ spectra are now all ≥ 0, showing considerable improvements for VIIRS ocean color products, particularly for biological and biogeochemical products (e.g., chlorophyll-a concentration, diffuse attenuation coefficient at 490 nm $K_d(490)$) that are derived using VIIRS $nL_w(\lambda)$ spectra. Several detailed examples from VIIRS measurements over various coastal and inland waters are provided and discussed. The new technique has been implemented in the Multi-Sensor Level-1 to Level-2 (MSL12) ocean color data processing system, which has been used for the routine production of VIIRS global ocean color products.**

***Index Terms*—Ocean color remote sensing, atmospheric correction, ocean optics, VIIRS**

I. Introduction

SINCE the success of the NASA Coastal Zone Color Scanner (CZCS) mission [1, 2], several ocean color satellite sensors capable of routine global coverage have been launched, e.g., the Sea-viewing Wide Field-of-view Sensor (SeaWiFS) (1997–2010) [3], the Moderate Resolution Imaging Spectroradiometer (MODIS) [4, 5] on the Terra (1999–present) and Aqua (2002–present) satellites, the Medium-Resolution Imaging Spectrometer (MERIS) [6] on the Envisat (2002–2012), the Visible Infrared Imaging Radiometer Suite (VIIRS) [7, 8] on the Suomi National Polar-orbiting Partnership (SNPP) (2011–present) and NOAA-20 (2017–present), the Ocean and Land Colour Instrument (OLCI) on the Sentinel-3A satellite (2016–present), and the Second-Generation Global Imager (SGLI) on the Global Change Observation Mission-Climate (GCOM-C) (2017–present). In fact, we now have an unprecedented view of ocean optical, biological, and biogeochemical properties on a global scale through the use of advanced algorithms to process satellite data [9].

For ocean color remote sensing, atmospheric correction is the key data processing procedure that removes radiance contributions from the atmosphere and ocean surface [10-12]. The purpose of atmospheric correction is to derive the normalized water-leaving radiance spectra $nL_w(\lambda)$ from the satellite-measured top-of-atmosphere (TOA) radiances [10-13]. Effectively, after carrying out atmospheric correction, satellite-derived $nL_w(\lambda)$ spectra should be the same as (or very close to) those measured directly on the ocean surface (e.g., from a ship) with assumptions of no atmosphere and the sun at nadir [10, 12, 14-16]. In the standard atmospheric correction algorithm, which has been used to routinely derive global ocean color products, the two near-infrared (NIR) bands (e.g., SeaWiFS 765 and 865 nm, MODIS 748 and 869 nm, and VIIRS 745 and 862 nm) are used to carry out atmospheric correction, i.e., to estimate aerosol radiance contributions, with the assumption of a black ocean at the two NIR bands (i.e., no NIR $nL_w(\lambda)$ contributions) [12]. This is after the correction of the Rayleigh-scattering radiance contributions from the satellite-measured TOA radiances [17-20]. The NIR black ocean assumption is generally valid for the open ocean with low chlorophyll-a (Chl-a) concentration [21]. However, for productive ocean waters and particularly over turbid coastal and inland waters, the ocean/water NIR $nL_w(\lambda)$ radiance contributions are no longer negligible, and can be very significant [21-25]. In these cases, the NIR atmospheric correction often results in significant errors in satellite-derived $nL_w(\lambda)$ spectra. Indeed, there have been continued efforts in the science community to account for the NIR ocean radiance contributions using the *Gordon and Wang* (1994) [10] standard NIR atmospheric correction algorithm [21-23, 26-29]. On the other hand, as an alternative (and better) approach for dealing with turbid coastal and inland

Submitted on 1/29/2018.

Menghua Wang (email: Menghua.Wang@noaa.gov) and Lide Jiang are both with the Center for Satellite Applications and Research, NESDIS/NOAA, 5830 University Research Court, College Park, MD 20746, USA. Lide Jiang is also affiliated with CIRA at Colorado State University, Fort Collins, CO 80523, USA.

waters, *Wang* (2007) [11] proposed atmospheric correction algorithms using the shortwave infrared (SWIR) bands utilizing the characteristics of much stronger water absorptions at the SWIR wavelengths, compared with those at the NIR bands [30]. Indeed, the black ocean assumption is generally valid at the SWIR bands even for highly turbid waters [31]. In fact, there are many studies and applications that use the SWIR- and NIR-SWIR-based atmospheric correction algorithms for satellite ocean color data processing over turbid coastal and inland waters [32-38].

Another big challenge in satellite ocean color remote sensing is handling the cases associated with the strongly absorbing aerosols [12, 39]. There are several regional studies for dealing with the absorbing aerosols in satellite ocean color remote sensing [40-43]. Although cases with strongly absorbing aerosols (e.g., dust, smoke, air pollution from nearby cities) can be detected [44], accurate correction of radiance contributions from strongly absorbing aerosols requires accurate aerosol vertical profile information [12, 39], which is typically not available over the global ocean. For cases with strongly absorbing aerosols, which are generally over coastal and inland waters, satellite-derived $nL_w(\lambda)$ spectra are usually biased low, in particular, for the short blue bands (e.g., at the VIIRS 410 nm) [12, 39], even with $nL_w(410) < 0$. Obviously, cases with VIIRS-derived $nL_w(410) < 0$ are unphysical, leading to significant errors (biased low) in $nL_w(\lambda)$ spectra as well as $nL_w(\lambda)$-derived water biological and biogeochemical products. It often results in null retrievals of Chl-a and $K_d(490)$ (the water diffuse attenuation coefficient at 490 nm), if both $nL_w(443)$ and $nL_w(486) < 0$ as these data are used for deriving Chl-a and $K_d(490)$ products [45, 46]. Therefore, it is desirable to make improvement in these cases for satellite ocean color remote sensing.

In this paper, we develop a technique to improve VIIRS-derived $nL_w(\lambda)$ spectra for the cases with $nL_w(410) < 0$, i.e., using information from VIIRS-measured $nL_w(\lambda)$ at the short blue band. This is because the shorter the wavelength at sensor-measured radiances [or derived $nL_w(\lambda)$], the more sensitive it is for detecting strongly absorbing aerosols [12, 39, 44], e.g., radiance at the ultraviolet (UV) wavelength is even better (more sensitive) for detecting absorbing aerosols. Specifically, using the *Gordon and Wang* (1994) [10] and *Wang* (2007) [11] atmospheric correction algorithms, the negative $nL_w(\lambda)$ always begins with the shortest wavelength and then progresses to the next shortest, etc., due to strongly spectral coherency in the error in satellite-derived $nL_w(\lambda)$ [12, 47], e.g., negative value starts with $nL_w(\lambda)$ at the VIIRS 410 nm, then 443 nm, 486 nm, etc. Thus, with the information of VIIRS-derived $nL_w(410) < 0$, further aerosol correction method can be carried out to make $nL_w(410) \geq 0$, removing unphysical retrievals for VIIRS-derived $nL_w(\lambda)$ spectra. Several detailed examples over coastal and inland waters are provided and discussed, showing that using the new technique VIIRS-derived ocean color products are improved for cases of strongly absorbing aerosols (e.g., dust, smoke, air pollution from nearby big cities), as well as some cases with waters containing high concentration of colored dissolved organic matter (CDOM) and extremely high concentration of total suspended mater (TSM), over coastal and inland waters.

II. Methodology

In this section, the approach to deal with the case of VIIRS-derived $nL_w(410) < 0$ over coastal and inland waters is outlined. Specifically, the Multi-Sensor Level-1 to Level-2 (MSL12) ocean color data processing system is described first. Next, the issue with the strongly absorbing aerosols is discussed. Finally, the new technique to improve satellite ocean color products using the information from VIIRS-derived $nL_w(410) < 0$ is described and outlined.

A. Satellite Ocean Color Data Processing System

The MSL12 ocean color data processing system is being used for processing VIIRS data from the Sensor Data Records (SDR or Level-1B data) to ocean color Environmental Data Records (EDR or Level-2 data) [8, 48]. In fact, MSL12 has been routinely producing VIIRS-NOAA-20 global ocean color products since its door open on December 13, 2017. MSL12 was actually developed for the purpose of using a consistent and common ocean color data processing system to process global ocean color data from multiple satellite ocean color sensors [49-51]. Specifically, MSL12 is based on the NASA SeaWiFS Data Analysis System (SeaDAS) version 4.6 with some important modifications, including the SWIR- and NIR-SWIR-based atmospheric correction algorithms for the improved satellite ocean color data over coastal and inland waters [11, 24, 52, 53]. It should be noted that for MSL12 the aerosol lookup tables (LUTs) were generated using the 12 aerosol models derived from the work of *Shettle and Fenn* (1979) [54]. Specifically, they are the Oceanic model with relative humidity (RH) of 99% (O99), the Maritime models with RH of 50%, 70%, 90%, 99% (M50, M70, M90, M99), the Coastal models with RH of 50%, 70%, 90%, 99%, (C50, C70, C90, C99), and the Tropospheric models with RH of 50%, 90%, 99% (T50, T90, T99) [10, 11, 54-56]. The aerosol LUTs contain the fitting coefficients for a large number of solar-sensor geometries and for aerosol optical thickness (AOT) values up to 0.8 [11]. It should be particularly noted that aerosol models used in MSL12 are non- or weakly absorbing. Specifically, the aerosol single-scattering albedo values for the aerosol models O99, M50–M99, C50–C99, and T50–T99 are 1.0, 0.982–0.999, 0.976–0.998, and 0.930–0.993, respectively. In addition, the same MSL12 has also been used to process ocean color products from MODIS and the Korean Geostationary Ocean Color Imager (GOCI) [57]. Certainly, MSL12 will be used for producing global ocean color products from all future VIIRS sensors onboard the Joint Polar Satellite System (JPSS) series, e.g., JPSS-2, JPSS-3, etc.

There are many studies and applications that use the SWIR-based ocean color data processing over extremely turbid coastal and inland waters [32-38]. In particular, to avoid the NIR saturation issue for extremely turbid waters [28, 58], the SWIR-based atmospheric correction algorithm must be used over turbid coastal and inland waters. However, over the global open ocean, the standard NIR atmospheric correction is still preferred due to the sensor performance noise error in the SWIR bands

[47, 59, 60]. In fact, results show that the NIR-SWIR combined atmospheric correction can produce the best ocean color products over global open oceans and coastal/inland waters [36, 52, 53]. Therefore, in this study, the NIR-SWIR-based atmospheric correction in MSL12 is used to derive all VIIRS data, as well as to develop a new approach for improved VIIRS ocean color products. It should be noted that, using the in situ optics data from the Marine Optical Buoy (MOBY) in the waters off Hawaii [61], the VIIRS on-orbit vicarious calibration was carried out to derive consistent calibration gain coefficients for the NIR-SWIR combined atmospheric correction [62].

B. Issues with Atmospheric Correction

The major and still outstanding issue with the current standard atmospheric correction is for cases with strongly absorbing aerosols [12], e.g., dust, smoke, air pollution from nearby major cities, etc. Strongly absorbing aerosols are characterized by their significantly low single-scattering albedo values, i.e., much less than 1. For example, dusts strongly absorb at the short blue wavelengths, while they are almost non-absorbing in the NIR and SWIR wavelengths [63]. In addition, dust particles are generally non-spherical, which has considerable impact on the satellite-measured back-scattering radiances [64, 65]. Since the TOA radiances reflected from strongly absorbing aerosols are significantly less than those from non- or weakly-absorbing aerosols, the standard atmospheric correction algorithm generally overestimates aerosol radiance contributions (i.e., subtraction of too much aerosol radiances), leading to underestimation of satellite-derived $nL_w(\lambda)$ spectra, in particular, for the short blue bands [12]. In fact, it often leads to negative $nL_w(\lambda)$ values at the short blue bands. These phenomena have been observed consistently in satellite ocean color measurements of SeaWiFS, MODIS, VIIRS, etc., particularly over coastal and inland waters. However, it should be noted that, in order to properly deal with strongly absorbing aerosols, one needs not only realistic absorbing aerosol models to build the aerosol LUTs, but also importantly accurate information of aerosol vertical locations (profiles) [12, 39], which are currently not available globally.

C. Atmospheric Correction Using $nL_w(\lambda)$ Information at the Short Blue Band

In the *Gordon and Wang* (1994) [10] NIR-based and *Wang* (2007) [11] SWIR-based atmospheric correction algorithms, the aerosol single-scattering epsilon value $\varepsilon(\lambda, \lambda_0)$, which is an aerosol parameter used for estimation of aerosol spectral radiance contributions [10-12, 66, 67], is inferred from the aerosol contributions of the two NIR or SWIR bands. Effectively, the single-scattering epsilon $\varepsilon(\lambda, \lambda_0)$ can be related to aerosol spectral reflectance contribution $\rho_A(\lambda)$ at visible bands and removed (or corrected for) there [10-12]. However, if such a calculation results in a negative $nL_w(410)$ (e.g., with cases of strongly absorbing aerosols), we can recalculate the aerosol radiance spectrum by forcing $nL_w(410)$ to be non-negative. Since generally there is no information about the true value of $nL_w(410)$, one can just force it to be zero, which is the minimal physically meaningful value. Thus, using the new (increased) $nL_w(410) = 0$ from the original $nL_w(410) < 0$, the reduced aerosol reflectance contribution at the wavelength of 410 nm, $\rho_A(410)$, can be recalculated [10, 11, 66]. We now have aerosol reflectance contributions at the short blue and NIR bands at 410 and 862 nm, and a new aerosol multiple-scattering epsilon value $\varepsilon^{(M)}(410, 862)$ [67] can be directly calculated using aerosol reflectance values at the 410 and 862 nm. Specifically, the new multiple-scattering epsilon $\varepsilon^{(M)}(410, 862)$ is estimated using the *Wang and Gordon* (1994) [66] approximation, i.e.,

$$\varepsilon^{(M)}(410, 862) = \exp[452 \times c(410, 862)], \quad (1)$$

where $c(410, 862)$ is a coefficient that is derived from aerosol radiances at the wavelengths of 410 and 862 nm [66, 67]. It should be noted that Eq. (1) is an approximation for computing the multiple-scattering epsilon $\varepsilon^{(M)}(410, 862)$ [10-12, 66, 67]. However, it is expected that this approximation does not significantly affect results when considering the large uncertainties from the assumption of nil $nL_w(410)$ value. From Eq. (1) with the new estimated $\varepsilon^{(M)}(410, 862)$ [i.e., $\rho_A(410)/\rho_A(862)$] from sensor-measured aerosol radiances at the short blue (assuming $nL_w(410) = 0$) and NIR bands, $\varepsilon^{(M)}(\lambda, 862)$ for any other bands between the 410 and 862 nm for VIIRS-SNPP can be calculated [66], i.e.,

$$\varepsilon^{(M)}(\lambda, 862) = \exp\left[(862 - \lambda) \times \frac{\ln\left(\varepsilon^{(M)}(410,862)\right)}{452}\right]. \quad (2)$$

Therefore, aerosol reflectance contributions from other bands can be recalculated using the new $\varepsilon^{(M)}(\lambda, 862)$ derived from Eq. (2), i.e.,

$$\rho_A(\lambda) = \varepsilon^{(M)}(\lambda, 862)\, \rho_A(862), \quad (3)$$

where $\rho_A(\lambda)$ and $\rho_A(862)$ are aerosol reflectances at the VIIRS wavelength λ and 862 nm [10-12], respectively. Aerosol reflectances for VIIRS-SNPP spectral bands at 410, 443, 486, 551, 638, 671, 745, and 862 nm can now be recomputed and subtracted, and finally revised $nL_w(\lambda)$ values can be derived (with assumption of $nL_w(410) = 0$).

Specifically, the new technique approach can be summarized as the following: (a) for cases (pixels) with $nL_w(410) < 0$, new $\varepsilon^{(M)}(410, 862)$ values are computed using Eqs. (1) and (2); (b) the new aerosol reflectance spectra are then re-calculated using Eq. (3) and subtracted, leading to the modified water-leaving radiance spectra; (c) using the re-calculated aerosol reflectance with assumptions of the same aerosol models as from the previous retrievals atmospheric diffuse transmittance values are recomputed; and (d) finally the new/correct $nL_w(\lambda)$ values are derived.

The above technique that uses the information of the VIIRS-derived $nL_w(410)$ for further improving ocean color products can be applied to the NIR-, SWIR-, and NIR-SWIR-based atmospheric correction algorithms. For the SWIR-based algorithms, the modification of $\varepsilon^{(M)}(\lambda, 862)$ for the case with $nL_w(410) < 0$ is the same as for the NIR atmospheric correction algorithm, i.e., the reference wavelength is still at the NIR 862 nm (not at the SWIR band). Thus, the implementation of the

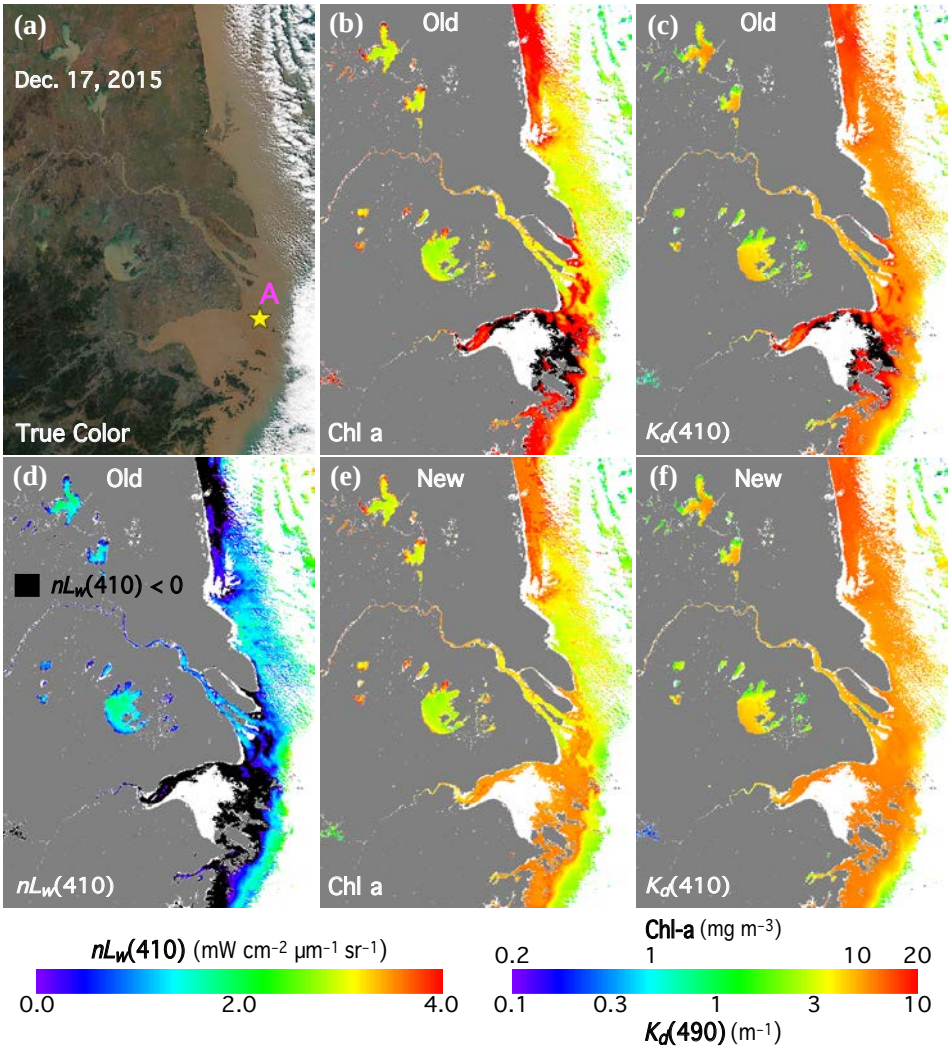

Fig. 1. Comparison of VIIRS-derived ocean color products before (old) and after applying the proposed correction (new) for the case over the China east coast acquired on December 17, 2015 at 4:54 UTC for VIIRS images of (a) true color, (b) old Chl-a, (c) old K_d(490), (d) old nL_w(410), (e) new Chl-a, and (f) new K_d(490). Location A is noted in Fig. 1(a) for further quantitative analysis.

proposed technique into MSL12 is relatively straightforward. It should be noted that the proposed technique does not make any assumption of what causing $nL_w(410) < 0$ and only uses the information of the negative radiance value at the short blue band. Thus, the new technique can be applied to any cases with $nL_w(410) < 0$.

III. Results from VIIRS Measurements

With the implemented new correction technique for dealing with negative nL_w(410) cases, which mostly happen over coastal and inland waters, some detailed case studies over various coastal and inland waters are provided in this section. In particular, results showing improvements in VIIRS ocean color products using the new scheme for dealing with the cases of $nL_w(410) < 0$ are provided and discussed. In the following sub-sections, six case studies in coastal and inland waters are presented, showing improvements after nL_w(410) was forced to a value of zero for pixels with the original $nL_w(410) < 0$. It is noted that all results presented here are derived using the NIR-SWIR combined atmospheric correction in MSL12.

A. China's East Coastal Region

China's east coast is one of the most turbid regions in the world [68]. Sometimes sediment-laden waters in the region get so turbid that it makes the NIR atmospheric correction invalid and it fails to get any retrievals [28, 58]. Fig. 1 presents an example of such a case, which was acquired on December 17, 2015 at 4:54 UTC by VIIRS-SNPP [true color image shown in Fig. 1(a)]. Location A marked in Fig. 1(a) is for further quantitative analysis later. By using the NIR-SWIR-based atmospheric correction [52], the SWIR-based atmospheric correction is automatically used for such turbid waters, thereby avoiding the NIR saturation issue [28, 58]. By examining the VIIRS-derived nL_w(410) data before applying the new proposed correction, the region of $nL_w(410) < 0$ is easily identified in Fig. 1(d) with the black masking (including the location A), which is the region where the proposed correction algorithm will be applied. In the VIIRS-derived ocean color products, such as Chl-a [Fig. 1(b)] and K_d(490) [Fig. 1(c)], there are no retrievals (masked in black) in the Hangzhou Bay region, and there are also significantly high values of Chl-a and K_d(490) around these

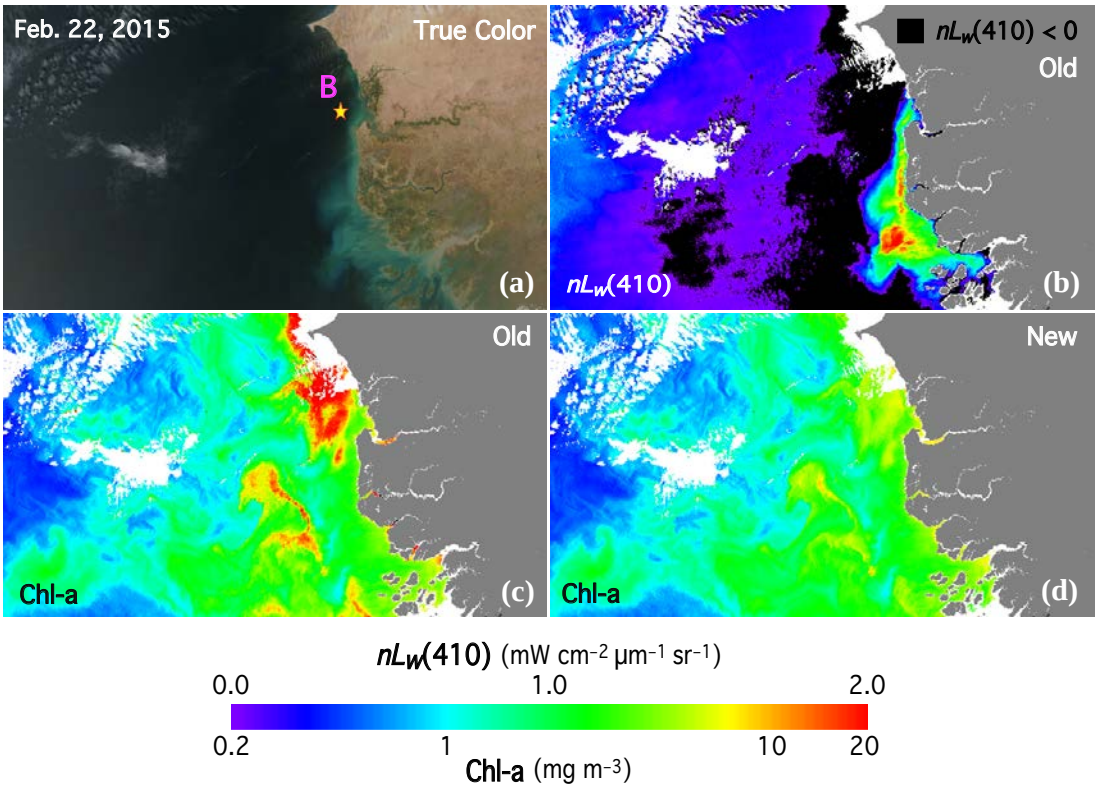

Fig. 2. Comparison of VIIRS-derived ocean color products before (old) and after applying the proposed correction (new) for the case over the west coast of North Africa acquired on February 22, 2015 at 14:48 UTC for VIIRS images of (a) true color, (b) old $nL_w(410)$, (c) old Chl-a, and (d) new Chl-a. Location B is noted in Fig. 2(a) for further quantitative analysis.

regions (values are obviously different from the nearby regions). The main reason for negative $nL_w(\lambda)$ values in this case is most likely due to non-negligible $nL_w(\lambda)$ at the VIIRS SWIR band 1238 nm used for the SWIR atmospheric correction in the Hangzhou Bay [31], and is probably not because of the strongly absorbing aerosols.

After applying the proposed correction, the first noticeable aspect is the recovery of the area that had previous algorithm failure in the VIIRS-derived ocean color products [Figs. 1(e) and 1(f)], as well as significantly changed values in the regions after the correction. Missing Chl-a data in Fig. 1(b) are now recovered along with significantly reduced values. New Chl-a values around the Hangzhou Bay are now improved [25] and consistent spatially (although may still have errors due to Chl-a algorithm issue for the region) compared with those from the original data in Fig. 1(b). It is also evident that Chl-a values around the Old Yellow River [region in the top of Figs. 1(b) and 1(e)] are also significantly reduced due to improved $nL_w(\lambda)$ at 443, 486, and 551 nm. For $K_d(490)$, the recovered values are quite consistent with the ambient values in the uncorrected region, including the coastal region and inland waters (e.g., Lake Taihu), which is quite encouraging [Fig. 1(f)]. It should be noted that the assumption of $nL_w(410) = 0$ is not likely to be correct (although $nL_w(410)$ usually is very low for highly turbid waters) and will have some impact on the VIIRS-derived $nL_w(\lambda)$ spectra. The impact is more on $nL_w(\lambda)$ at the short wavelengths than those on the longer ones. Therefore, the recovered and corrected Chl-a data may have slightly more impact than $K_d(490)$, as the Chl-a algorithm uses $nL_w(\lambda)$ at the blue and green bands [45], while the $K_d(490)$ algorithm uses $nL_w(\lambda)$ at the green and red bands for turbid coastal and inland waters [46]. However, compared to the original results, there are obvious improvements in VIIRS ocean color products after applying the proposed correction.

B. West Coast of the Sahara Desert

The west coast of North Africa is frequently impacted by dust storms from the Sahara Desert. Fig. 2(a) shows a VIIRS true color image acquired on February 22, 2015 at 14:48 UTC. Location B is noted in Fig. 2(a) for further quantitative analysis. This is a typical case of negative $nL_w(410)$ due to strongly absorbing aerosols from desert dust because the water off the North Africa coast is generally not very turbid. In addition, the presence of dust aerosols in the region from VIIRS true color images in the previous days (not shown) is confirmed. In the original VIIRS-derived $nL_w(410)$ image before the new correction was applied, a very large area with negative $nL_w(410)$ (masked in black) is easily identifiable offshore of the coastal plume [Fig. 2(b)]. The corresponding (original) Chl-a image in Fig. 2(c) shows a considerably overestimated Chl-a value (> ~20 mg m^{-3}) in the offshore of the coastal plume. After applying the proposed correction, Chl-a values in the region are much reduced and consistent with the ambient values (~5 mg m^{-3}) [Fig. 2(d)]. Therefore, with the new correction for the dust contaminated west coast of the Sahara Desert, VIIRS-derived Chl-a data are significantly improved.

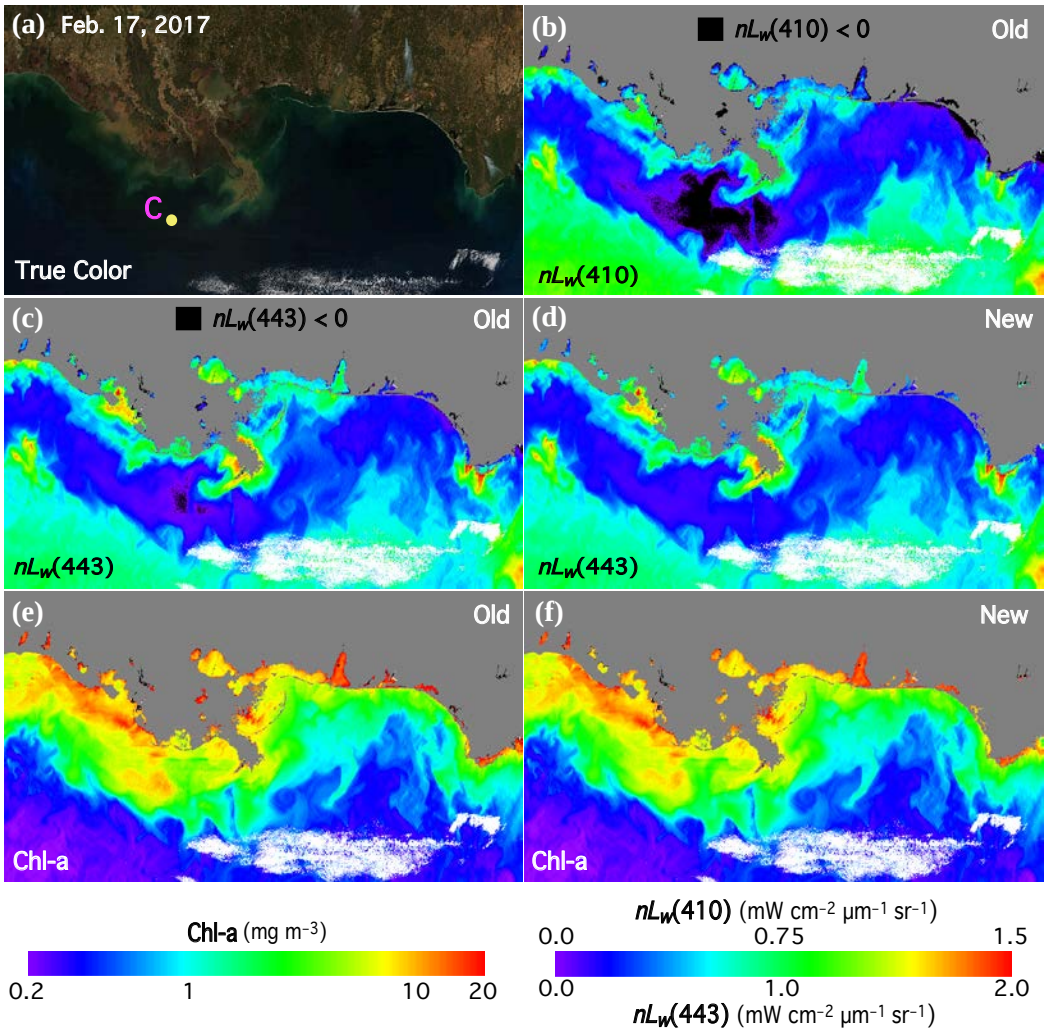

Fig. 3. Comparison of VIIRS-derived ocean color products before (old) and after applying the proposed correction (new) for the case over the coastal area in the northern Gulf of Mexico acquired on February 17, 2016 at 19:02 UTC for VIIRS images of (a) true color, (b) old $nL_w(410)$, (c) old $nL_w(443)$, (d) new $nL_w(443)$, (e) old Chl-a, and (f) new Chl-a. Location C is noted in Fig. 3(a) for further quantitative analysis.

C. *The Northern Gulf of Mexico*

Near the coastal area in the northern Gulf of Mexico (Fig. 3), the water mass may contain a high concentration of CDOM, and thus becomes so-called "black water" [69], which has strong absorption at the short blue wavelengths and leads to very low $nL_w(\lambda)$ at VIIRS short blue bands. From the VIIRS true color image acquired on February 17, 2016 at 19:02 UTC, two sources of smoke can be identified [Fig. 3(a)]. In addition, dozens of wildfire spots in the nearby land region on the previous days are also observed from VIIRS true color images. Location C is noted in Fig. 3(a) for further quantitative analysis later. The already low $nL_w(410)$ due to high CDOM concentration in the region is superimposed by the absorbing aerosol effect from smoke and shows negative $nL_w(410)$ values in the coastal water off the Louisiana coast, as well as several inland lakes and bays along the coast [Fig. 3(b)]. In fact, some regions even have negative $nL_w(443)$ [Fig. 3(c)]. Furthermore, in those inland lakes and bays, the Chl-a algorithm either fails or retrieves unreasonably high Chl-a values due to negative or significantly underestimated $nL_w(\lambda)$ values at the blue bands. After applying the proposed correction, all missing pixels are recovered, e.g., $nL_w(443)$ data in Fig. 3(d). Values in the VIIRS-derived $nL_w(443)$ are also increased as expected [Fig. 3(d)] compared with the original values [Fig. 3(c)]. This leads to a reduced Chl-a value [Fig. 3(f)], in particular, over several inland lakes in the region (visually observable), compared with those from the original Chl-a data [Fig. 3(e)].

D. *West Coast of Southern Chile*

In Fig. 4, a portion along Chile's southern coastline was acquired by VIIRS-SNPP on October 18, 2016 at 19:05 UTC. VIIRS-derived $nL_w(\lambda)$ values at VIIRS short blue band 410 nm [Fig. 4(b)] and blue at 443 nm (not shown) both show negative retrievals near the coastline and inside of the estuary, resulting in the failed Chl-a retrievals or abnormally high Chl-a values (> ~100 mg m^{-3}) [Fig. 4(c)] in these locations, e.g., location D noted in Fig. 4(a) has Chl-a value of 324.6 mg m^{-3} in the original Chl-a data [Fig. 4(c)]. After applying the proposed correction, new Chl-a retrievals are recovered at the originally failed locations and Chl-a values are significantly reduced, e.g., the new Chl-a value at location D in Fig. 4(a) is now 2.69 mg m^{-3}, which is quite reasonable. It is important to note that after the correction Chl-a data over estuaries in the region are

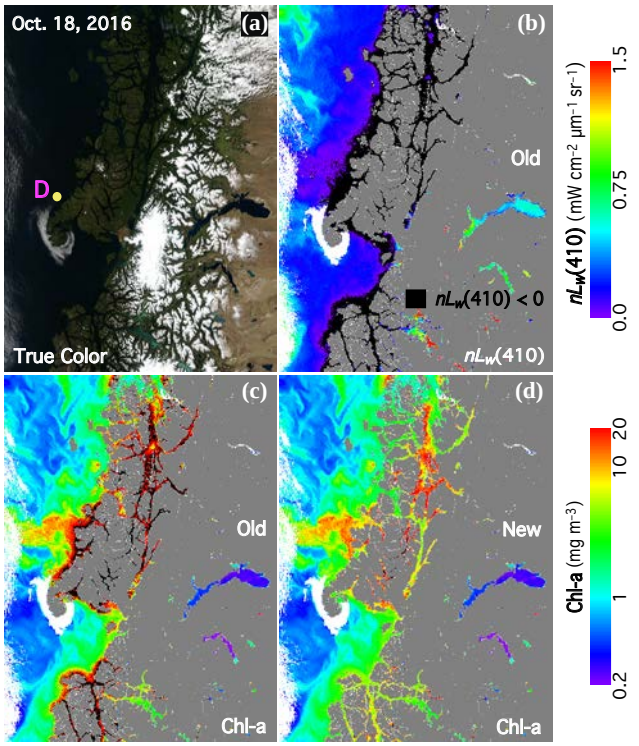

Fig. 4. Comparison of VIIRS-derived ocean color products before (old) and after (new) applying the proposed correction for the case over the west coast of the southern Chile acquired on October 18, 2016 at 19:05 UTC for VIIRS images of (a) true color, (b) old $nL_w(410)$, (c) old Chl-a, and (d) new Chl-a. Location D is noted in Fig. 4(a) for further quantitative analysis.

dramatically reduced and are more consistent with values in the nearby regions, e.g., comparing Chl-a values between Fig. 4(c) and Fig. 4(d) for the estuary regions located at the bottom of the images.

E. The Great Lakes

The Great Lakes are the world's largest inland bodies of water by their total area, and Fig. 5 shows a snapshot of VIIRS images acquired on June 29, 2015 at 18:37 UTC. During that period, there was an extensive Canadian wildfire and thick smoke extended from northwest Canada to west of the Great Lakes area, observable from the same day true color image (not shown). An extended area including most of Lake Ontario and a portion of Lake Huron shows negative $nL_w(\lambda)$ retrievals at VIIRS 410 nm and even at the 443 nm band [Figs. 5(b) and 5(c)], and also shows the corresponding significantly elevated Chl-a concentration in the region [Fig. 5(e)], e.g., the location E marked in Fig. 5(a) had Chl-a value of 228.6 mg m^{-3} using the original data processing. After applying the correction, the Chl-a concentration at those locations now has reasonable values, e.g., Chl-a value in the location E noted in Fig. 5(a) is now reduced to 2.7 mg m^{-3} [Fig. 5(f)]. In fact, after applying the correction, the new Chl-a data over the entirety of Lake Erie are more consistent and relatively uniform [Fig. 5(f)], compared to those in the original data [Fig. 5(e)]. Chl-a values in the other $nL_w(410) < 0$ regions shown in Fig. 5(b), e.g., the North Channel and Georgian Bay in Lake Huron, are also significantly reduced and now quite reasonable after the correction [Fig. 5(f)]. It is also quite obvious that ocean color products are significantly improved in Lake Simcoe after applying the correction, e.g., with improved $nL_w(443)$ (increased from the negative values) [Fig. 5(d)] and significantly reduced and now reasonable Chl-a data [Fig. 5(f)].

F. The Black Sea

Acquired on April 6, 2016 at 10:20 UTC, VIIRS captured an event of extended dust contamination region in the Black Sea [Fig. 6(a)]. In Fig. 6(a), VIIRS true color image for the next day on April 7, 2016 is also presented, confirming significant dust contamination in the region. Fig. 6(b) shows large negative $nL_w(410)$ over an extended region in the Black Sea, with also negative $nL_w(443)$ over some areas. Indeed, the presence of dust over the area was clearly observable from the VIIRS true color image on the next day of April 7, 2016 [Fig. 6(a)]. After applying the correction, there are increases in VIIRS-derived $nL_w(\lambda)$ spectra for all visible bands, e.g., $nL_w(443)$ and $nL_w(551)$ in Figs. 6(d) and (f) compared with those in Figs. 6(c) and (e). In fact, after the correction at the location F marked in Fig. 6(a), VIIRS-derived $nL_w(\lambda)$ at wavelengths of 410, 443, 486, 551, 638, 671, and 745 nm are increased from the original values of –0.31, 0.08, 0.33, 0.21, 0.03, 0.01, and 0. mW cm^{-2} μm^{-1} sr^{-1} to 0., 0.43, 0.67, 0.46, 0.18, 0.13, and 0.05 mW cm^{-2} μm^{-1} sr^{-1}, respectively. Chl-a and $K_d(490)$ values in the location F change slightly from the original 0.74 mg m^{-3} and 0.10 m^{-1} to 0.86 mg m^{-3} and 0.11 m^{-1}, respectively.

G. Some Quantitative Evaluations

In order to further understand the performance of the proposed correction method, some quantitative evaluations were carried out for the cases discussed in the previous sections. Specifically, VIIRS ocean color data derived from locations A to F noted in the corresponding Figs. 1(a) to 6(a) were selected to have further detailed analysis. The original VIIRS-derived ocean color products have significant errors in all these six locations. Fig. 7 shows quantitative comparisons in VIIRS-derived $nL_w(\lambda)$ spectra before (old) and after (new) the proposed correction is applied for cases at the locations of A to F corresponding to Figs. 1(a) to 6(a), respectively. Obviously, after applying the correction, VIIRS-derived $nL_w(\lambda)$ spectra are increased and all values are now positive (red curves in Fig. 7), compared to those from the original $nL_w(\lambda)$ spectra (blue curves in Fig. 7). Some quantitative comparison values in $nL_w(486)$, $nL_w(551)$, ratio $nL_w(486)/nL_w(551)$, Chl-a, and $K_d(490)$ before (old) and after (new) applying the proposed correction for these six cases are summarized in Table I. In addition, monthly median values for these five ocean color products, which were derived from the corresponding month for the specific VIIRS measurement day (e.g., December 2015 for the case of Fig. 1), are also included for comparison in Table I. The monthly $nL_w(486)/nL_w(551)$ ratio values in Table I are calculated using the monthly median $nL_w(\lambda)$ data. It is noted that for absorbing aerosol cases, e.g., Fig. 6, it is difficult to find nearby clear days for new ocean color data evaluations. Thus, monthly data are used. Monthly median (instead of mean) values, which are computed with excluding all $nL_w(410) < 0$ cases, usually reflect

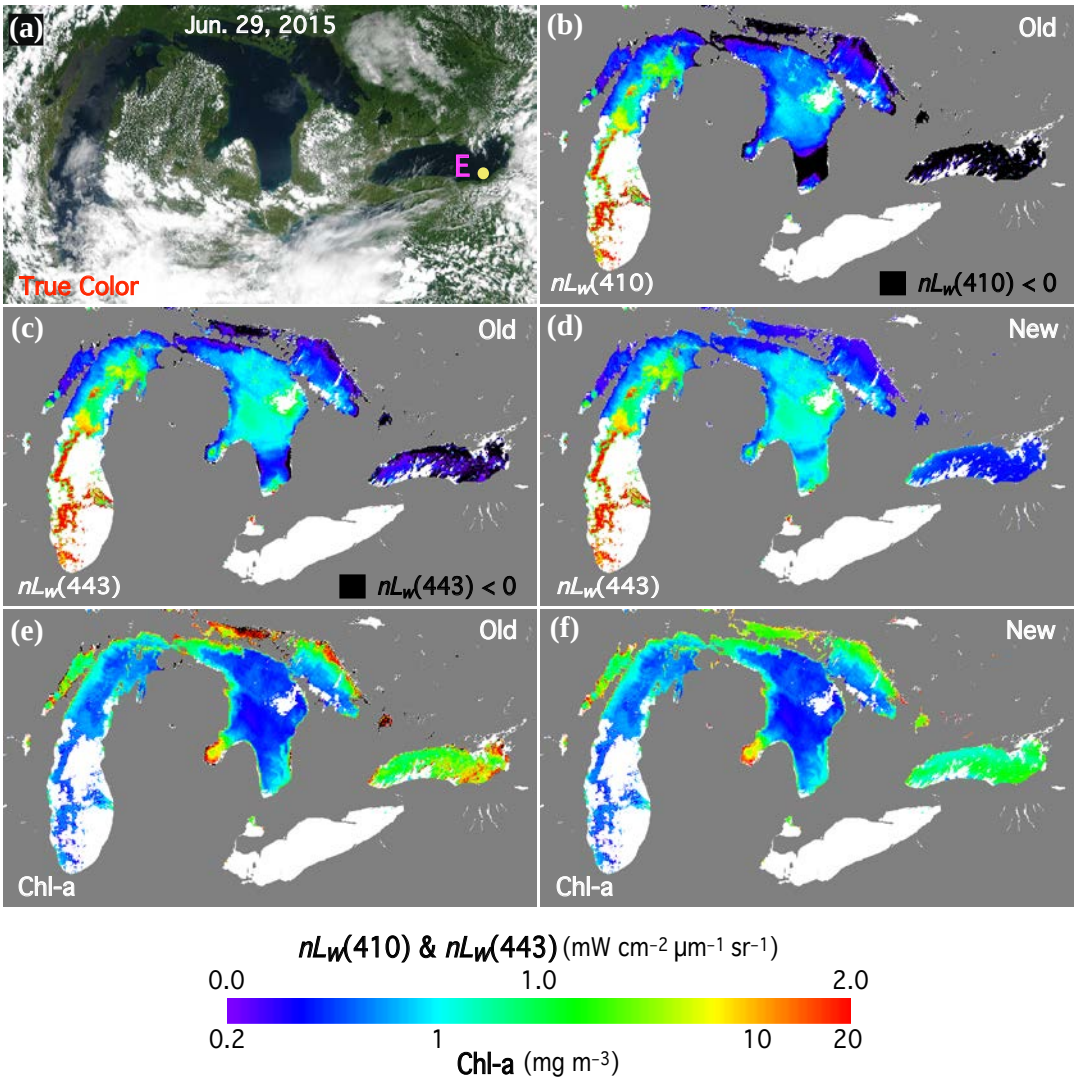

Fig. 5. Comparison of VIIRS-derived ocean color products before (old) and after applying the proposed correction (new) for the case over the Great Lakes acquired on June 29, 2015 at 18:37 UTC for VIIRS images of (a) true color, (b) old $nL_w(410)$, (c) old $nL_w(443)$, (d) new $nL_w(443)$, (e) old Chl-a, and (f) new Chl-a. Location E is noted in Fig. 5(a) for further quantitative analysis.

typical values in normal conditions and are less impacted by outliers.

Specifically, Fig. 7(a) shows VIIRS-derived $nL_w(\lambda)$ spectra at the location A (30.71°N, 122.16°E) in Fig. 1(a) with the peak at the red band 638 nm of ~6.0 mW cm^{-2} μm^{-1} sr^{-1}, showing characteristics of sediment-dominated (extremely) turbid waters. The $nL_w(\lambda)$ at the NIR band 862 nm also reached an extremely high value of 2.7 mW cm^{-2} μm^{-1} sr^{-1} [Fig. 7(a)]. There are some slightly negative $nL_w(410)$ (relative to overall high $nL_w(\lambda)$ spectra) in the region from the original retrievals [Figs. 1(b) and 7(a)]. This is likely due to non-black pixel at the VIIRS SWIR 1238 nm band for such extremely turbid waters [31], as well as the SWIR noise effects [59]. After applying the proposed correction, the $nL_w(\lambda)$ spectrum is all elevated [Fig. 7(a)], removing unphysical $nL_w(410) < 0$ cases, and therefore their values are much closer to those from monthly data derived in December 2015 (Table I). Specifically, compared to the monthly data, the relative differences for $nL_w(486)$, $nL_w(551)$, Chl-a, and $K_d(490)$ are reduced from about –30.2%, –11.6%, 196.6%, and 40.0% in the original data to about –6.0%, –0.4%, 57.2%, and 25.4% in the new improved data, respectively. It should be noted that the monthly data are certainly not the truth for the VIIRS data measured at a specific day due to temporal variation. However, they can be used to indicate which data are more reasonable and accurate. The analysis and evaluation for the case in Figs. 1 and 7(a) demonstrate that the proposed correction can indeed improve VIIRS ocean color products over extremely turbid waters.

Fig. 7(b) compares VIIRS-derived $nL_w(\lambda)$ spectra before (old) and after (new) the proposed correction for the location B (13.48°N, 17.16°W) in Fig. 2(a). The $nL_w(\lambda)$ spectra are peaked at the green band at 551 nm. The region was contaminated by the Sahara dust, leading to the negative $nL_w(\lambda)$ at both 410 and 443 nm bands [Fig. 7(b)]. After applying the correction, the $nL_w(\lambda)$ spectrum is obviously improved, showing that the differences relative to the February 2015 monthly median values reduced from about –61.9%, –29.8%, 1035.2%, and 125.3% to about –4.8%, 1.8%, 50.0%, and 34.5% in Table I for

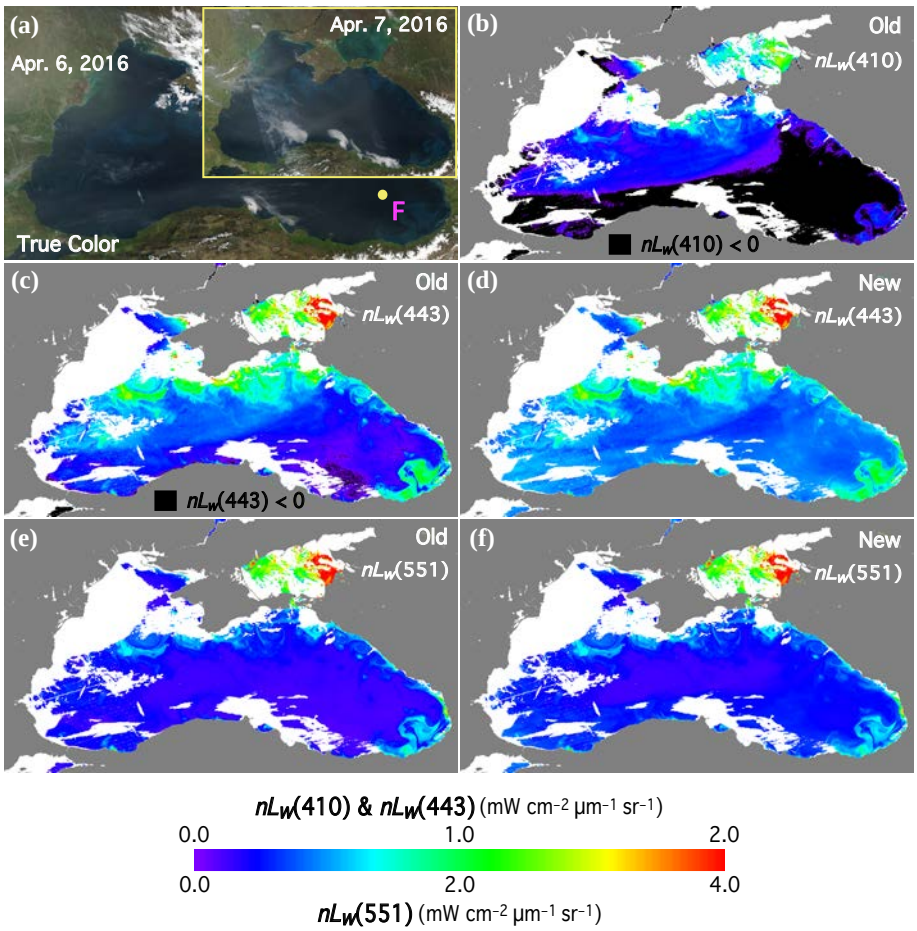

Fig. 6. Comparison of VIIRS-derived ocean color products before (old) and after applying the proposed correction (new) for the case over the Black Sea acquired on April 6, 2016 at 10:20 UTC for VIIRS images of (a) true color, (b) old $nL_w(410)$, (c) old $nL_w(443)$, (d) new $nL_w(443)$, (e) old $nL_w(551)$, and (f) new $nL_w(551)$. Location F is noted in Fig. 6(a) for further quantitative analysis. Note that VIIRS true color image acquired on April 7, 2017 is also shown in Fig. 6(a).

$nL_w(486)$, $nL_w(551)$, Chl-a, and $K_d(490)$, respectively. It is particularly noted that for the Chl-a improvement, i.e., after applying the correction, the Chl-a value is now quite reasonable. Other cases shown in Figs. 7(c)–(f) corresponding to the locations of C (28.56°N, 90.48°W), D (46.36°S, 75.33°W), E (43.39°N, 75.03°W), and F (42.31°N, 39.41°E) also have obvious improvements in ocean color products after applying the correction. As results shown in Table I, the differences relative to the corresponding monthly median data for $nL_w(486)$ are reduced from about –53.5%, –87.5%, –81.8%, and –57.7% to about –9.3%, –12.5%, 13.6%, and –14.1%, respectively, while differences for $nL_w(551)$ are reduced from about –35.0%, –56.5%, –37.0%, and –54.3% to about –10.0%, 0.%, 19.6%, and 0.%, respectively. After applying the correction, Chl-a data improvements are quite obvious, in particular, for some unreasonably very high values, e.g., the location B in Fig. 2(a) Chl-a reduced from 42.57 to 5.62 mg m^{-1}, location D in Fig. 4(a) Chl-a reduced from 324.60 to 2.69 mg m^{-1}, and location E in Fig. 5(a) Chl-a reduced from 228.60 to 2.70 mg m^{-1}. In addition, the new Chl-a data are more consistent spatially with those from the nearby regions and temporally with those from the nearby days (e.g., from monthly comparison results). The new $K_d(490)$ data also show some obvious improvements, e.g., spatially for the case in Fig. 1 for the highly turbid China's east coast region, and temporally $K_d(490)$ values are more consistent with the monthly median data in Table I. Specifically, comparing to the monthly median $K_d(490)$ values, the differences in $K_d(490)$ for the locations A to F in Figs. 1(a) to 6(a) are changed from the original 40.0%, 125.3%, 52.9%, 392.3%, 500.0%, and 25.0% to about 25.4%, 34.5%, 32.4%, 3.8%, 10.5%, and 37.5%, respectively. It is noted that for the case of the location F in Fig. 6(a), the $K_d(490)$ difference compared with the monthly value is slightly increased, which may be due to high temporal variation for the region. Both Chl-a and $K_d(490)$ data improvements are actually reflected in the improvements of radiance ratio $nL_w(486)$/$nL_w(551)$ in Table I. Indeed, compared to the monthly median values (Table I), the differences in the ratio $nL_w(486)/nL_w(551)$ for the location A to F in Figs. 1(a) to 6(a) are changed (mostly improved) from the original –21.7%, –48.0%, –27.8%, –76.4%, –72.9%, and –8.8% to about –5.0%, –6.7%, 0.%, –11.8%, –6.3%, and –14.7%, respectively.

IV. Discussion

Using the information from the cases with VIIRS-derived $nL_w(410) < 0$, which are unphysical, a technique has been

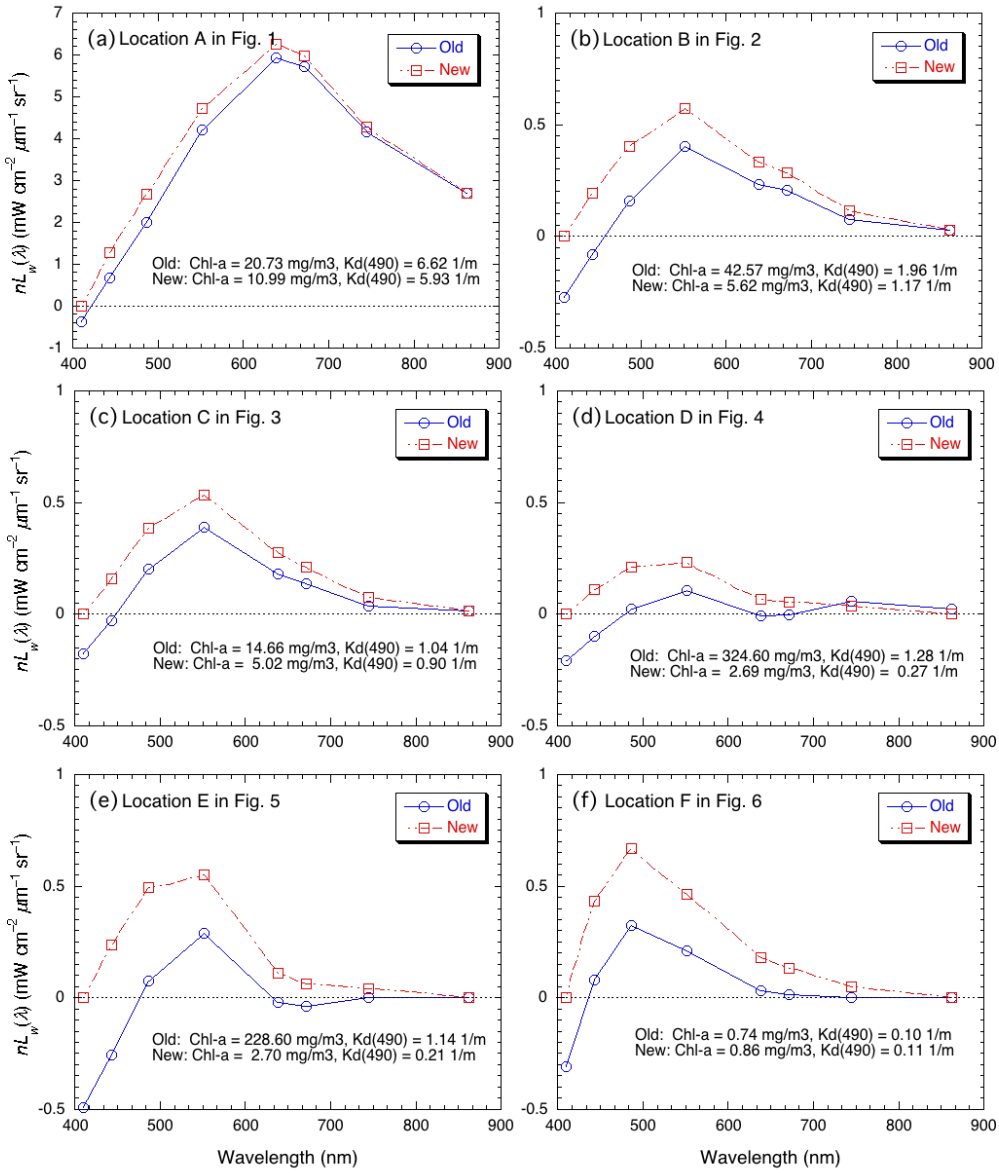

Fig. 7. Quantitative comparison of VIIRS-derived $nL_w(\lambda)$ spectra before (old in blue) and after applying the proposed correction (new in red) for the cases of (a) location A in Fig. 1(a), (b) location B in Fig. 2(a), (c) location C in Fig. 3(a), (d) location D in Fig. 4(a), (e) location E in Fig. 5(a), and (f) location F in Fig. 6(a). Chl-a and $K_d(490)$ values (old and new) for the study locations are also noted in each plot for comparison.

developed to improve VIIRS ocean color products by forcing $nL_w(410) = 0$. Essentially, because $nL_w(410)$ is generally unknown, the black pixel is assumed for $nL_w(410)$ in the new technique for further improvement of VIIRS-derived ocean color products. Cases with VIIRS-derived $nL_w(410) < 0$ usually occur with strongly absorbing aerosols, e.g., dust, smoke, air pollution from nearby cities, etc., which are generally in coastal and inland waters. However, slightly negative $nL_w(410)$ cases may also appear for high CDOM-dominated waters where $nL_w(410)$ is indeed close to zero (i.e., black waters [69]) due to atmospheric correction errors (e.g., noise error may make $nL_w(410)$ slightly lower than 0). For such cases (e.g., CDOM-dominated waters), the assumption of the black pixel at 410 nm band [i.e., zero $nL_w(410)$] is reasonable. In addition, for very extremely turbid waters (e.g., extremely high TSM waters), it may also cause $nL_w(410) < 0$ because of the issue with non-black pixels at the VIIRS SWIR 1238 nm band [31]. For all these $nL_w(410) < 0$ cases, which usually happen in coastal and inland water regions, the proposed technique improves VIIRS ocean color products. In fact, the new correction technique has been implemented in MSL12 ocean color data processing system for routinely producing VIIRS global ocean color products. It should be emphasized that the new correction technique does not make any assumptions about atmospheric conditions or water types. It only uses the information about negative $nL_w(\lambda)$ value at the short blue band, and the correction is only applied to those pixies with $nL_w(410) < 0$.

In addition to the above mention $nL_w(410) < 0$ cases, some recent studies [70, 71] also showed that the land adjacent effects may also lead to the negative $nL_w(\lambda)$ at the blue wavelengths

TABLE I. COMPARISONS OF VIIRS-DERIVED $nL_w(\lambda)$ AT 486 AND 551 NM, RATIO OF $nL_w(486)/nL_w(551)$, CHL-A, AND $K_d(490)$ AT THE LOCATIONS A–F NOTED IN FIGS. 1(a)–6(a) FROM CASES OF BEFORE AND AFTER APPLYING THE PROPOSED CORRECTION. THE MONTHLY MEDIAN VALUES CORRESPONDING TO THE SPECIFIC MONTH FOR THESE CASES ARE ALSO LISTED.

Location	Case	$nL_w(486)^{\dagger}$	$nL_w(551)^{\dagger}$	$nL_w(486)/nL_w(551)$	Chl-a‡	$K_d(490)^{*}$
A in Fig. 1(a)	Before	1.99	4.20	0.47	20.73	6.62
	After	2.68	4.73	0.57	10.99	5.93
	Monthly	2.85	4.75	0.60	6.99	4.73
B in Fig. 2(a)	Before	0.16	0.40	0.39	42.57	1.96
	After	0.40	0.58	0.70	5.62	1.17
	Monthly	0.42	0.57	0.75	3.75	0.87
C in Fig. 3(a)	Before	0.20	0.39	0.52	14.66	1.04
	After	0.39	0.54	0.72	5.02	0.90
	Monthly	0.43	0.60	0.72	4.91	0.68
D in Fig. 4(a)	Before	0.03	0.10	0.24	324.60	1.28
	After	0.21	0.23	0.90	2.69	0.27
	Monthly	0.24	0.23	1.02	2.16	0.26
E in Fig. 5(a)	Before	0.08	0.29	0.26	228.60	1.14
	After	0.50	0.55	0.90	2.70	0.21
	Monthly	0.44	0.46	0.96	2.06	0.19
F in Fig. 6(a)	Before	0.33	0.21	1.55	0.74	0.10
	After	0.67	0.46	1.45	0.86	0.11
	Monthly	0.78	0.46	1.70	0.51	0.08

†Unit of mW cm^{-2} μm^{-1} sr^{-1} ‡Unit of mg m^{-3} *Unit of m^{-1}

from satellite measurements. Furthermore, for pixels nearby clouds, the cloud shadowing effects will lead to biased low satellite-derived $nL_w(\lambda)$ spectra, and may even go negative for $nL_w(\lambda)$ at the blue bands [72]. For all these cases (if these cases are not properly flagged and masked), the proposed technique will improve satellite-derived ocean color products, as there is no assumption of which case for applying the new correction.

It is noted that *He et al.* (2012) [73] also proposed an atmospheric correction approach by assuming the black pixel at the UV band to correct for the NIR $nL_w(\lambda)$ contributions over turbid waters. In fact, the key implementation component of the *He et al.* (2012) algorithm [73] and the correction technique proposed in this study is similar, i.e., using the *Wang and Gordon* (1994) [66] formulation for recalculating the aerosol multiple-scattering epsilon value and aerosol spectral reflectance contributions. However, *He et al.* (2012) [73] assume the NIR $nL_w(\lambda)$ is incorrect and use the zero UV $nL_w(\lambda)$ assumption (i.e., the black pixel assumption at the UV band), while the approach proposed in this study uses the known information of $nL_w(\lambda)$ at the short blue band (i.e., $nL_w(410) < 0$) and assumes the NIR $nL_w(\lambda)$ is correct. Indeed, results from this study show that the proposed approach using the $nL_w(410) < 0$ information improved VIIRS-SNPP ocean color products with increased $nL_w(\lambda)$ spectra for those unphysical retrievals.

Indeed, from the case studies using the proposed correction technique, it is found that in every case the $nL_w(\lambda)$ spectra are elevated and improved. Certainly, there are still uncertainties. The uncertainties are mainly from three sources. The first one is the assumed $nL_w(410)$ value used in the correction scheme. This is the major uncertainty for the technique. In this study, zero (black) $nL_w(410)$ is used for all the cases, but in reality $nL_w(410)$ can be any non-negative value. If *a priori* knowledge of the true $nL_w(410)$ values are available, especially in regional studies [74], these known $nL_w(410)$ values can be used in the proposed correction technique to further improve satellite-derived ocean color products. The second source of uncertainty comes from the reference wavelength the correction scheme is based on, i.e., the reliability of $nL_w(862)$ derived from the original atmospheric correction. The error from the $nL_w(862)$ estimation propagates to shorter wavelengths through the new estimated epsilon value. In such a case, using the red band or even the green band as the reference wavelength may improve the result if we have confidence in their $nL_w(\lambda)$ values derived from the original algorithm. The third source of uncertainty is from the correction scheme itself by assuming the *Wang and Gordon* (1994) [66] single-scattering epsilon in replace of multiple-scattering epsilon [67] in estimation of the aerosol radiance spectrum [Eqs. (1) and (2)]. However, based on results from our further investigation in this study (not shown), the difference between using such a simple approximation and the original aerosol model approach is usually much smaller than the other two types of uncertainties, particularly uncertainty from the assumed $nL_w(410)$ value. Therefore, the primary uncertainty for the new technique is indeed from the uncertainty of the new $nL_w(410)$ value used in the proposed correction.

Although uncertainties exist in the new VIIRS-derived $nL_w(\lambda)$ spectra, results from various study cases show that the new $nL_w(\lambda)$-derived ocean biological and biogeochemical products, e.g., Chl-a and $K_d(490)$, are significantly improved. This is mainly because errors in satellite-derived $nL_w(\lambda)$ are strongly spectrally coherent [12, 47], and errors are reduced significantly using $nL_w(\lambda)$ ratio algorithms for Chl-a [45] and $K_d(490)$ [46]. Table I lists the Chl-a and $K_d(490)$ values corresponding to the $nL_w(\lambda)$ spectra shown in Fig. 7 and in almost all cases the correction scheme improved the Chl-a and $K_d(490)$ products. In addition, using the new correction, the data coverage from VIIRS-derived ocean color products is also increased significantly, in particular, over coastal and inland waters. Previously missing data due to the negative $nL_w(410)$ issue are now recovered with consistent values in the nearby

regions. Thus, it is emphasized that the objective of this study is really for the improvement of satellite-derived ocean color products (removal unphysical retrievals) using the new proposed technique over global coastal and inland waters.

On the other hand, it is recognized that, although the proposed correction scheme generally works well to improve VIIRS ocean color products over strongly absorbing aerosols in global coastal and inland waters, it is more or less like a practical and patchwork approach. Ideally, to fundamentally resolve the issue with the strongly absorbing aerosols in ocean color remote sensing, we should still pursue for the methodology of identifying absorbing aerosols [44] and then using realistic absorbing aerosol models (i.e., realistic aerosol LUTs) with accurate aerosol vertical profile information for atmospheric correction.

V. Conclusion

Using the VIIRS-derived negative $nL_w(410)$ information, a new technique has been developed to improve satellite-measured ocean color products by forcing the $nL_w(410) = 0$, and then re-deriving aerosol reflectance contributions in visible wavelengths. Effectively, VIIRS-derived $nL_w(\lambda)$ spectra are elevated using the newly proposed correction and removed for unphysical (i.e., negative) $nL_w(\lambda)$ at short blue and blue bands. Most of these negative $nL_w(410)$ cases are associated with the strongly absorbing aerosols, e.g., dust, smoke, air pollution from nearby cities, etc., and some are related to strongly CDOM-dominated waters or extremely high TSM-dominated waters. Generally, they are all located over coastal and inland water regions. Examples of six VIIRS cases over various coastal and inland water regions are studied using the new proposed correction method. Results show that in all of these cases VIIRS-derived ocean color products are improved after applying the new correction method, in particular, for Chl-a and $K_d(490)$ products that are derived using the $nL_w(\lambda)$ ratio algorithms. In addition, data coverage from VIIRS-SNPP measurements is also considerably increased over global coastal and inland waters. The new correction technique can further improve satellite-derived ocean color products if the true $nL_w(410)$ values are known, e.g., for regional applications with known $nL_w(410)$ information from in situ data (or known from historical knowledge). The new correction scheme has been implemented in MSL12 for routine production of VIIRS global ocean color products. However, it should be noted that, in order to properly deal with the strongly absorbing aerosols for satellite ocean color remote sensing, realistic absorbing aerosol models and accurate aerosol vertical profile information are necessary.

Acknowledgment

This research was supported by the Joint Polar Satellite System (JPSS) funding and NOAA Product Development, Readiness, and Application (PDRA)/Ocean Remote Sensing (ORS) Program funding. The VIIRS global daily true color and ocean color data imageries, as well as calibration/validation results, can be found at the NOAA Ocean Color Team website (https://www.star.nesdis.noaa.gov/sod/mecb/color/) and VIIRS mission-long ocean color data are freely available through the NOAA CoastWatch website (https://coastwatch.noaa.gov/). We thank three anonymous reviewers for their useful comments. The views, opinions, and findings contained in this paper are those of the authors and should not be construed as an official NOAA or U.S. Government position, policy, or decision.

References

[1] H. R. Gordon, D. K. Clark, J. L. Mueller, and W. A. Hovis, "Phytoplankton Pigments from the Nimbus-7 Coastal Zone Color Scanner: Comparisons with Surface Measurements," *Science*, vol. 210, pp. 63–66, 1980.

[2] W. A. Hovis, D. K. Clark, F. Anderson, R. W. Austin, W. H. Wilson, E. T. Baker, D. Ball, H. R. Gordon, J. L. Mueller, S. T. E. Sayed, B. Strum, R. C. Wrigley, and C. S. Yentsch, "Nimbus 7 Coastal Zone Color Scanner: system description and initial imagery," *Science*, vol. 210, pp. 60–63, 1980.

[3] C. R. McClain, G. C. Feldman, and S. B. Hooker, "An overview of the SeaWiFS project and strategies for producing a climate research quality global ocean bio-optical time series," *Deep Sea Res. Part II*, vol. 51, pp. 5–42, 2004.

[4] V. V. Salomonson, W. L. Barnes, P. W. Maymon, H. E. Montgomery, and H. Ostrow, "MODIS: advanced facility instrument for studies of the Earth as a system," *IEEE Trans. Geosci. Remote Sens.*, vol. 27, pp. 145–153, 1989.

[5] W. E. Esaias, M. R. Abbott, I. Barton, O. B. Brown, J. W. Campbell, K. L. Carder, D. K. Clark, R. L. Evans, F. E. Hodge, H. R. Gordon, W. P. Balch, R. Letelier, and P. J. Minnet, "An overview of MODIS capabilities for ocean science observations," *IEEE Trans. Geosci. Remote Sens.*, vol. 36, pp. 1250–1265, 1998.

[6] M. Rast, J. L. Bezy, and S. Bruzzi, "The ESA Medium Resolution Imaging Spectrometer MERIS a review of the instrument and its mission," *Int. J. Remote Sens.*, vol. 20, pp. 1681–1702, 1999.

[7] M. D. Goldberg, H. Kilcoyne, H. Cikanek, and A. Mehta, "Joint Polar Satellite System: The United States next generation civilian polar-orbiting environmental satellite system," *J. Geophys. Res. Atmos.*, vol. 118, pp. 13463–13475, doi: 10.1002/2013JD020389, 2013.

[8] M. Wang, X. Liu, L. Tan, L. Jiang, S. Son, W. Shi, K. Rausch, and K. Voss, "Impact of VIIRS SDR performance on ocean color products," *J. Geophys. Res. Atmos.*, vol. 118, pp. 10347–10360, doi:10.1002/jgrd.50793, 2013.

[9] C. R. McClain, "A decade of satellite ocean color observations," *Annu. Rev. Mar. Sci.*, vol. 1, pp. 19–42, 2009.

[10] H. R. Gordon and M. Wang, "Retrieval of water-leaving radiance and aerosol optical thickness over the oceans with SeaWiFS: A preliminary algorithm," *Appl. Opt.*, vol. 33, pp. 443–452, 1994.

[11] M. Wang, "Remote sensing of the ocean contributions from ultraviolet to near-infrared using the shortwave infrared bands: simulations," *Appl. Opt.*, vol. 46, pp. 1535–1547, 2007.

[12] IOCCG, "Atmospheric Correction for Remotely-Sensed Ocean-Colour Products," in *Reports of the International Ocean-Colour Coordinating Group*, vol. No. 10, M. Wang, Ed. IOCCG, Dartmouth, Canada, 2010.

[13] D. Antoine and A. Morel, "A multiple scattering algorithm for atmospheric correction of remotely sensed ocean colour (MERIS instrument): principle and implementation for atmospheres carrying various aerosols including absorbing ones," *Int. J. Remote Sens.*, vol. 20, pp. 1875–1916, 1999.

[14] A. Morel and G. Gentili, "Diffuse reflectance of oceanic waters. III. Implication of bidirectionality for the remote-sensing problem," *Appl. Opt.*, vol. 35, pp. 4850–4862, 1996.

[15] H. R. Gordon, "Normalized water-leaving radiance: revisiting the influence of surface roughness," *Appl. Opt.*, vol. 44, pp. 241–248, 2005.

[16] M. Wang, "Effects of ocean surface reflectance variation with solar elevation on normalized water-leaving radiance," *Appl. Opt.*, vol. 45, pp. 4122–4128, 2006.

[17] H. R. Gordon, J. W. Brown, and R. H. Evans, "Exact Rayleigh scattering calculations for use with the Nimbus-7 Coastal Zone Color Scanner," *Appl. Opt.*, vol. 27, pp. 862–871, 1988.

[18] M. Wang, "The Rayleigh lookup tables for the SeaWiFS data processing: Accounting for the effects of ocean surface roughness," *Int. J. Remote Sens.*, vol. 23, pp. 2693–2702, 2002.
[19] M. Wang, "A refinement for the Rayleigh radiance computation with variation of the atmospheric pressure," *Int. J. Remote Sens.*, vol. 26, pp. 5651–5663, 2005.
[20] M. Wang, "Rayleigh radiance computations for satellite remote sensing: Accounting for the effect of sensor spectral response function," *Opt. Express*, vol. 24, pp. 12414–12429, 2016.
[21] D. A. Siegel, M. Wang, S. Maritorena, and W. Robinson, "Atmospheric correction of satellite ocean color imagery: the black pixel assumption," *Appl. Opt.*, vol. 39, pp. 3582–3591, 2000.
[22] K. G. Ruddick, F. Ovidio, and M. Rijkeboer, "Atmospheric correction of SeaWiFS imagery for turbid coastal and inland waters," *Appl. Opt.*, vol. 39, pp. 897–912, 2000.
[23] S. J. Lavender, M. H. Pinkerton, G. F. Moore, J. Aiken, and D. Blondeau-Patissier, "Modification to the atmospheric correction of SeaWiFS ocean color images over turbid waters," *Cont. Shelf Res.*, vol. 25, pp. 539–555, 2005.
[24] M. Wang and W. Shi, "Estimation of ocean contribution at the MODIS near-infrared wavelengths along the east coast of the U.S.: Two case studies," *Geophys. Res. Lett.*, vol. 32, L13606, doi:10.1029/2005GL022917, 2005.
[25] M. Wang, J. Tang, and W. Shi, "MODIS-derived ocean color products along the China east coastal region," *Geophy. Res. Lett.*, vol. 34, L06611, doi:10.1029/2006GL028599, 2007.
[26] R. P. Stumpf, R. A. Arnone, R. W. Gould, P. M. Martinolich, and V. Ransibrahmanakul, "A partially coupled ocean-atmosphere model for retrieval of water-leaving radiance from SeaWiFS in coastal waters," NASA Goddard Space Flight Center, Greenbelt, Maryland, SeaWiFS Postlaunch Technical Report Series Vol. 22, NASA Tech. Memo. 2003-206892, S. B. Hooker and E. R. Firestone, Eds., 2003.
[27] S. W. Bailey, B. A. Franz, and P. J. Werdell, "Estimation of near-infrared water-leaving reflectance for satellite ocean color data processing," *Opt. Express*, vol. 18, pp. 7521–7527, 2010.
[28] L. Jiang and M. Wang, "Improved near-infrared ocean reflectance correction algorithm for satellite ocean color data processing," *Opt. Express*, vol. 22, pp. 21657–21678, 2014.
[29] M. Wang, W. Shi, and L. Jiang, "Atmospheric correction using near-infrared bands for satellite ocean color data processing in the turbid western Pacific region," *Opt. Express*, vol. 20, pp. 741–753, doi:10.1364/oe.20.000741, 2012.
[30] G. M. Hale and M. R. Querry, "Optical constants of water in the 200nm to 200µm wavelength region," *Appl. Opt.*, vol. 12, pp. 555–563, 1973.
[31] W. Shi and M. Wang, "An assessment of the black ocean pixel assumption for MODIS SWIR bands," *Remote Sens. Environ.*, vol. 113, pp. 1587–1597, 2009.
[32] W. Shi and M. Wang, "Satellite observations of flood-driven Mississippi River plume in the spring of 2008," *Geophy. Res. Lett.*, vol. 36, L07607, doi:10.1029/2009GL037210, 2009.
[33] W. Shi and M. Wang, "Satellite observations of the seasonal sediment plume in central East China Sea," *J. Mar. Syst.*, vol. 82, pp. 280–285, 2010.
[34] M. Wang, W. Shi, and J. Tang, "Water property monitoring and assessment for China's inland Lake Taihu from MODIS-Aqua measurements," *Remote Sens. Environ.*, vol. 115, pp. 841–854, 2011.
[35] M. Wang, C. J. Nim, S. Son, and W. Shi, "Characterization of turbidity in Florida's Lake Okeechobee and Caloosahatchee and St. Lucie estuaries using MODIS-Aqua measurements," *Water Research*, vol. 46, pp. 5410–5422, 2012.
[36] S. Son and M. Wang, "Water properties in Chesapeake Bay from MODIS-Aqua measurements," *Remote Sens. Environ.*, vol. 123, pp. 163–174, 2012.
[37] W. Shi and M. Wang, "Satellite views of the Bohai Sea, Yellow Sea, and East China Sea," *Prog. Oceanogr.*, vol. 104, pp. 35–45, 2012.
[38] W. Shi and M. Wang, "Characterization of particle backscattering of global highly turbid waters from VIIRS ocean color observations," *J. Geophys. Res. Oceans*, vol. 122, pp. 9255–9275, doi:10.1002/2017JC013191, 2017.
[39] H. R. Gordon, "Atmospheric correction of ocean color imagery in the Earth Observing System era," *J. Geophys. Res.*, vol. 102, pp. 17081–17106, 1997.
[40] R. Chomko and H. R. Gordon, "Atmospheric correction of ocean color imagery: use of the Junge power-law aerosol size distribution with variable refractive index to handle aerosol absorption," *Appl. Opt.*, vol. 37, pp. 5560–5572, 1998.
[41] C. Moulin, H. R. Gordon, R. M. Chomko, V. F. Banzon, and R. H. Evans, "Atmospheric correction of ocean color imagery through thick layers of Saharan dust," *Geophys. Res. Letters*, vol. 28, pp. 5–8, 2001.
[42] J. Brajard, C. Jamet, C. Moulin, and S. Thiria, "Use of a neuro-variational inversion for retrieving oceanic and atmospheric constituents from satellite ocean color sensor: Application to absorbing aerosols," *Neural Networks*, vol. 19, pp. 178–185, 2006.
[43] V. F. Banzon, H. R. Gordon, C. P. Kuchinke, D. Antoine, K. J. Voss, and R. H. Evans, "Validation of a SeaWiFS dust-correction methodology in the Mediterranean Sea: Identification of an algorithm-switching criterion," *Remote Sens. Environ.*, vol. 113, pp. 2689–2700, 2009.
[44] W. Shi and M. Wang, "Detection of turbid waters and absorbing aerosols for the MODIS ocean color data processing," *Remote Sens. Environ.*, vol. 110, pp. 149–161, 2007.
[45] J. E. O'Reilly, S. Maritorena, B. G. Mitchell, D. A. Siegel, K. L. Carder, S. A. Garver, M. Kahru, and C. R. McClain, "Ocean color chlorophyll algorithms for SeaWiFS," *J. Geophys. Res.*, vol. 103, pp. 24937–24953, 1998.
[46] M. Wang, S. Son, and J. L. W. Harding, "Retrieval of diffuse attenuation coefficient in the Chesapeake Bay and turbid ocean regions for satellite ocean color applications," *J. Geophys. Res.*, vol. 114, C10011, doi:10.1029/2009JC005286, 2009.
[47] M. Wang and H. R. Gordon, "Sensor performance requirements for atmospheric correction of satellite ocean color remote sensing," *Opt. Express*, vol. 26, pp. 7390–7403, 2018.
[48] M. Wang, L. Jiang, X. Liu, S. Son, J. Sun, W. Shi, L. Tan, K. Mikelsons, X. Wang, and V. Lance, "VIIRS ocean color products: A progress update," *Proc. the IEEE Int. Geosci. Remote Sens. Symposium (IGARSS)*, pp. 5848–5851, Beijing, China, July 10-15, http://dx.doi.org/10.1109/IGARSS.2016.7730528, 2016.
[49] M. Wang, "A sensitivity study of SeaWiFS atmospheric correction algorithm: Effects of spectral band variations," *Remote Sens. Environ.*, vol. 67, pp. 348–359, 1999.
[50] M. Wang and B. A. Franz, "Comparing the ocean color measurements between MOS and SeaWiFS: A vicarious intercalibration approach for MOS," *IEEE Trans. Geosci. Remote Sens.*, vol. 38, pp. 184–197, 2000.
[51] M. Wang, A. Isaacman, B. A. Franz, and C. R. McClain, "Ocean color optical property data derived from the Japanese Ocean Color and Temperature Scanner and the French Polarization and Directionality of the Earth's Reflectances: A comparison study," *Appl. Opt.*, vol. 41, pp. 974–990, 2002.
[52] M. Wang and W. Shi, "The NIR-SWIR combined atmospheric correction approach for MODIS ocean color data processing," *Opt. Express*, vol. 15, pp. 15722–15733, doi:10.1364/oe.15.015722, 2007.
[53] M. Wang, S. Son, and W. Shi, "Evaluation of MODIS SWIR and NIR-SWIR atmospheric correction algorithm using SeaBASS data," *Remote Sens. Environ.*, vol. 113, pp. 635–644, 2009.
[54] E. P. Shettle and R. W. Fenn, "Models for the Aerosols of the Lower Atmosphere and the Effects of Humidity Variations on Their Optical Properties," U.S. Air Force Geophysics Laboratory, Hanscom Air Force Base, Mass. AFGL-TR-79-0214, 1979.
[55] M. Wang, K. D. Knobelspiesse, and C. R. McClain, "Study of the Sea-Viewing Wide Field-of-View Sensor (SeaWiFS) aerosol optical property data over ocean in combination with the ocean color products," *J. Geophys. Res.*, vol. 110, D10S06, doi:10.1029/2004JD004950, 2005.
[56] M. Wang and H. R. Gordon, "Estimating aerosol optical properties over the oceans with the Multiangle Imaging SpectroRadiometer: some preliminary studies," *Appl. Opt.*, vol. 33, pp. 4042–4057, 1994.
[57] M. Wang, J. H. Ahn, L. Jiang, W. Shi, S. Son, Y. J. Park, and J. H. Ryu, "Ocean color products from the Korean Geostationary Ocean Color Imager (GOCI)," *Opt. Express*, vol. 21, pp. 3835–3849, 2013.
[58] W. Shi and M. Wang, "Ocean reflectance spectra at the red, near-infrared, and shortwave infrared from highly turbid waters: A study in the Bohai Sea, Yellow Sea, and East China Sea," *Limnol. Oceanogr.*, vol. 59, pp. 427–444, 2014.
[59] M. Wang and W. Shi, "Sensor noise effects of the SWIR bands on MODIS-derived ocean color products," *IEEE Trans. Geosci. Remote Sens.*, vol. 50, pp. 3280–3292, 2012.
[60] P. J. Werdell, B. A. Franz, and S. W. Bailey, "Evaluation of shortwave infrared atmospheric correction for ocean color remote sensing of Chesapeake Bay," *Remote Sens. Environ.*, vol. 114, pp. 2238–2247, 2010.

[61] D. K. Clark, H. R. Gordon, K. J. Voss, Y. Ge, W. Broenkow, and C. Trees, "Validation of atmospheric correction over the ocean," *J. Geophys. Res.*, vol. 102, pp. 17209–17217, 1997.
[62] M. Wang, W. Shi, L. Jiang, and K. Voss, "NIR- and SWIR-based on-orbit vicarious calibrations for satellite ocean color sensors," *Opt. Express*, vol. 24, pp. 20437–20453, 2016.
[63] O. Dubovik, B. N. Holben, T. F. Eck, A. Smirnov, Y. J. Kaufman, M. D. King, D. Tanre, and I. Slutsker, "Variability of absorption and optical properties of key aerosol types observed in worldwide locations," *J. Atmos. Sci.*, vol. 59, pp. 590–608, 2002.
[64] O. Dubovik, B. N. Holben, T. Lapyonok, A. Sinyuk, M. Mishchenko, P. Yang, and I. Slutsker, "Non-spherical aerosol retrieval method employing light scattering by spheroids," *Geophy. Res. Lett.*, vol. 29, pp. 1451, doi:10.1029/2001GL014506, 2002.
[65] O. Dubovik, A. Sinyuk, T. Lapyonok, B. N. Holben, M. Mishchenko, P. Yang, T. F. Eck, H. Volten, O. Munoz, B. Veihelmann, W. J. v. d. Zande, J.-F. Leon, M. Sorokin, and I. Slutsker, "Application of spheroid models to account for aerosol particle nonsphericity in remote sensing of desert dust," *J. Geophys. Res.*, vol. 111, D11208, doi:10.1029/2005JD006619, 2006.
[66] M. Wang and H. R. Gordon, "A simple, moderately accurate, atmospheric correction algorithm for SeaWiFS," *Remote Sens. Environ.*, vol. 50, pp. 231–239, 1994.
[67] M. Wang, "Extrapolation of the aerosol reflectance from the near-infrared to the visible: the single-scattering epsilon vs multiple-scattering epsilon method," *Int. J. Remote Sens.*, vol. 25, pp. 3637–3650, 2004.
[68] W. Shi and M. Wang, "Characterization of global ocean turbidity from Moderate Resolution Imaging Spectroradiometer ocean color observations," *J. Geophys. Res.*, vol. 115, C11022, doi:10.1029/2010JC006160, 2010.
[69] C. Hu, F. E. Muller-Karger, G. A. Vargo, M. B. Neely, and E. Johns, "Linkages between coastal runoff and the Florida Keys ecosystem: A study of a dark plume event," *Geophy. Res. Lett.*, vol. 31, L15307, doi:10.1029/2004GL020382, 2004.
[70] B. Bulgarelli, V. Kiselev, and G. Zibordi, "Simulation and analysis of adjacency effects in coastal waters: a case study," *Appl. Opt.*, vol. 53, pp. 1523–1545, 2014.
[71] B. Bulgarelli, V. Kiselev, and G. Zibordi, "Adjacency effects in satellite radiometric products from coastal waters: a theoretical analysis for the northern Adriatic Sea," *Appl. Opt.*, vol. 56, pp. 854–869, 2017.
[72] L. Jiang and M. Wang, "Identification of pixels with stray light and cloud shadow contaminations in the satellite ocean color data processing," *Appl. Opt.*, vol. 52, pp. 6757–6770, 2013.
[73] X. He, Y. Bai, D. Pan, J. Tang, and D. Wang, "Atmospheric correction of satellite ocean color imagery using the ultraviolet wavelength for highly turbid waters," *Opt. Express*, vol. 20, pp. 20754–20770, 2012.
[74] M. Oo, M. Vargas, A. Gilerson, B. Gross, F. Moshary, and S. Ahmed, "Improving atmospheric correction for highly productive coastal waters using the short wave infrared retrieval algorithm with water-leaving reflectance constraints at 412 nm," *Appl. Opt.*, vol. 47, pp. 3846–3859, 2008.

Menghua Wang received the B.S. degree in physics from Zhejiang University, Hangzhou, China, in 1982, the M.S. degree in physics (with distinction) from California State University, Northridge, CA, USA, in 1987, and the Ph.D. degree in physics from University of Miami, Coral Gables, FL, USA, in 1991.

Since January of 2005, he has been with the Center for Satellite Applications and Research (STAR), National Environmental Satellite, Data, and Information Service, National Oceanic and Atmospheric Administration, College Park, MD, USA, where he has been the Chief of the Marine Ecosystems and Climate Branch since 2010. His research experiences include radiative transfer modeling, ocean color remote sensing, remote retrievals and in situ measurements of aerosol and cloud optical and microphysical properties, development of calibration and validation techniques, and development of strategy and techniques for the data processing and data merging from the multiple ocean color sensors, development of the end-to-end satellite ocean color data processing system, and various applications in open ocean and coastal/inland water regions using satellite and in situ measurements.

Lide Jiang received the B.E. degree in electronic and information engineering from the Shanghai Jiao-Tong University, Shanghai, China, in 2002 and the Ph.D. degree in oceanography from University of Delaware, Newark, Delaware, in 2009.

He is currently a research scientist with the Center for Satellite Applications and Research, NOAA National Environmental Satellite, Data, and Information Service, College Park, Maryland and the Cooperative Institute for Research in Atmosphere (CIRA), Colorado State University, Fort Collins. His research interests are ocean color remote sensing and related algorithm development, implementation and real-world application for various ocean color sensors (MODIS-Aqua, VIIRS-SNPP and GOCI-COMS, etc.), including atmospheric correction, straylight identification, satellite data processing, and product development.